 doi:10.20944/preprints201804.0105.v1

# Using Dielectric Relaxation Spectroscopy to Characterize the Glass Transition and Onset of Crystallinity of Skim-Milk Powder

Martin G. Buehler, Fellow, IEEE, mgbuehler@earthlink.net
METER Group, Inc. 2365 NE Hopkins Ct., Pullman, WA 99163
Phone: 509-332-2756 Fax: 509-332-5158

**Abstract:** This paper describes the dielectric relaxation spectroscopy (DRS) method for obtaining glass transition temperature and the onset of crystallinity of skim milk powder (SMP). The methodology consists of exposing SMP samples to numerous constant temperatures, $T$, and water activities, $a_w$, and measuring the relaxation time. Measurements are based on changes in the loss-tangent height at its peak frequency. Glass transition times are identified at peaks in the loss-tangent height versus time curve and the onset of crystallinity times are identified when the loss-tangent height collapses. The analysis leads to two boundary curves: glass transition $T_g$, $a_w$ curve and the onset of crystallinity $T_c$, $a_w$ curve. They separate the SMP stable (long shelf life) and unstable (short shelf life) regions. Two curve fitting algorithms were developed for (a) $a_w^2$, $t_g$ curve where $t_g$ is the time to glass transition and $a_w^2$, $t_c$ curve where time $t_c$ is the time to onset of crystallinity and (b) $T_g$, $a_w$ and $T_c$, $a_w$ boundary curves. Finally, the DRS data are compared to differential scanning calorimetry (DSC) results.

Key Words: DRS dielectric relaxation, DSC differential scanning calorimetry, SMP skim milk powder, boundary curves.

**Introduction:** It is important to develop simple methods for characterizing skim-milk powder (SMP) because there is a need for dry milk which can be stored for several years, used for emergencies and is viable in hot regions of the earth [1]. With a world population of 7.6 billion people in 2017, the need for measurements ensuring the quality and shelf life of dry milk is growing since the world population is expected to reach 8.6 billion by 2030 [2]. The current annual world-wide production of SMP is 5 million tons [3].

SMP is produced by spray drying and so starts out in the amorphous or glassy state. In this state the SMP is hydroscopic and absorbs water. When exposed to the environmental variables, temperature ($T$) and water activity ($a_w$), it goes through glass transition and enters the rubbery state. Finally, the SMP enters the crystalline state where it is hydrophobic and desorbs water [1].

The glass transition of SMP has been extensively studied by Roos [4] and the crystallization of SMP was summarized most recently by Clark et.al [5]. Both authors used Differential Scanning Calorimetry (DSC). The addition to characterizing SMP using Dielectric Relaxation Spectroscopy (DRS) another purpose of this effort is to compare the DSC and DRS method. Differences between the methods are: (a) Non-zero heating rate is required for the DSC method; whereas, the DRS method can operate at a zero-heating rate or constant temperature. (b) The $a_w$ environment in the DSC method is not fixed for after samples are humidified using saturated salts they are encapsulated during DSC measurements; whereas, in the DRS method the $a_w$ environment is controlled in real time. (c) $a_w$ values for the DSC method are limited to the availability of saturated salts; whereas, the DRS method can operate between 0.05 and 0.95 $a_w$. Both

Preprints (www.preprints.org) | NOT PEER-REVIEWED | Posted: 9 April 2018 doi:10.20944/preprints201804.0105.v1

methods identify the glass transition temperature, $T_g$, at a given $a_w$. These results lead to differences in the $T_g$, $a_w$ boundary curves that divide SMP stable and unstable regions. These differences are import in shelf-life predictions.

The SMP crystalline state was characterized using the DRS method and is based on catastrophic changes in measured properties. The characterization identifies the time to onset of crystallinity and leads to the crystallization temperature, $T_c$ at a given $a_w$. These values appear in the $T_c$, $a_w$ state diagram and show that the crystallinity $T_c$, $a_w$ curve lies above the glass transition $T_g$, $a_w$ curve.

**Experimental Details:** In characterizing the phase change in SMP, a one-gram sample was placed in a 3-cm diameter test cell. The certificate of analysis for this sample indicates it consists of 0.77% Fat, 3.11% Moisture, 7.77% Ash, 34.64% Protein and 52.71% Carbohydrate. In this paper the measurements characterize the SMP carbohydrates. The test cell has buried interdigitated electrodes which produce electric fringe-fields that penetrate the sample [6]. The SMP was characterized using a Gamry Ref 600 Impedance Spectrometer measures the samples' impedance magnitude, |Z| and the phase angle, θ, at selected frequencies *f*. Measured values were acquired between 1 MHz and 0.01 Hz with five-points per decade. Each spectrum took about 20 minutes to acquire. The measurement time, $t_m$, was determined at the end of each spectrum. The sample environment can be controlled between 15°C and 60°C and between 0.05 and 0.95 $a_w$. Further description of the apparatus is presented elsewhere [7].

A typical temperature and $a_w$ profile is shown in Fig. 1. Each sample is given a preconditioning step consisting of 30°C and 0.30 $a_w$ where the preconditioning time $t_p$ is about 2.5 h. After $t_p$, the STP environment is shifted to the test phase at 45°C and 0.50 $a_w$ as illustrated in Fig. 1.

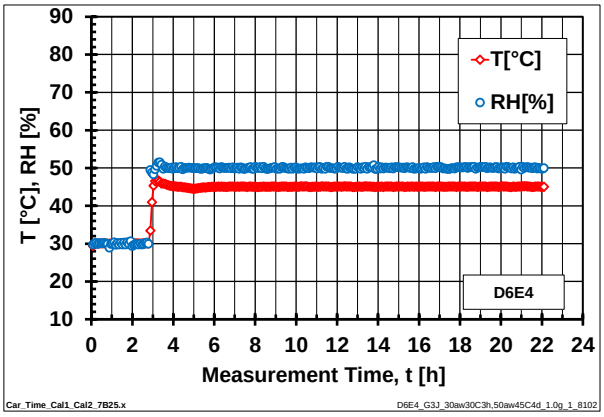


Fig. 1. After the preconditioning step, the test phase begins at 45°C and 0.50 $a_w$ where RH = 100$a_w$.

**Data Acquisition:** During the test phase, the sample relaxes as shown by the shift in the spectra in Fig. 2. This figure shows that that θ initially shifts to higher frequencies and then drops as the sample transforms to the crystalline phase. The spectra in Fig. 2a is analyzed by determining the peak height at the peak frequency by fitting five points about the peak with a parabola. The θ values in Fig. 2a were then converted to the loss-tangent values shown in Fig. 2b using $\tan\delta = \cot(-\theta)$ where θ as seen in Fig, 2a is negative. The loss-tangent height at the peak frequency is $\tan\delta_p$. The loss tangent, $\tan\delta = \varepsilon''/\varepsilon'$, is the ratio of the imaginary permittivity, $\varepsilon''$, to the real permittivity, $\varepsilon'$. The $\varepsilon''$ is the lossy part of the permittivity that describes the energy required to bring the dipoles found a critical frequency range in-line with the externally imposed AC electric field. The $\varepsilon'$ is the non-lossy part of the permittivity and accounts

*Preprints* (www.preprints.org) | NOT PEER-REVIEWED | Posted: 9 April 2018 doi:10.20944/preprints201804.0105.v1

for the dipoles outside the critical frequency range that cannot follow the externally imposed AC electric field. [8]. The critical frequencies are found in the vicinity of the peak in the $\varepsilon''$, f curve.

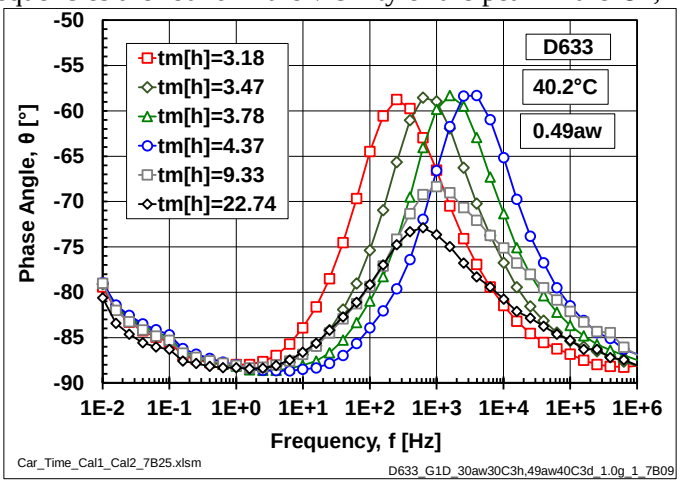


Fig. 2a. Phase angles measured at 40.2°C and 0.49 $a_w$ as the SMP relaxes.

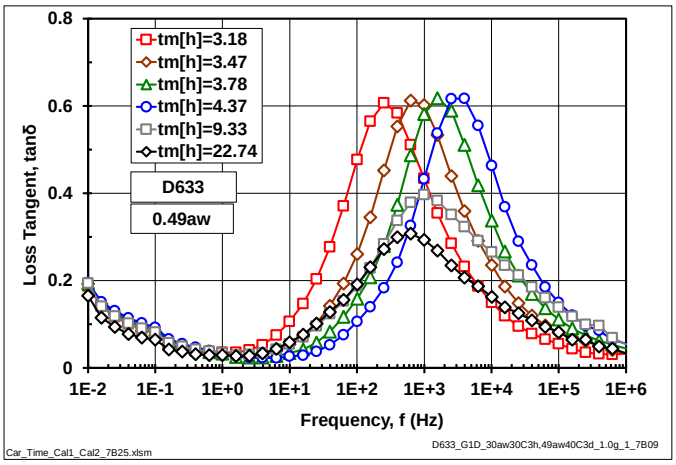


Fig. 2b. Loss tangent derived from the data in Fig. 2a.

Typical tan$\delta_p$, $t_m$ curves, in Fig. 3, show that the SMP collapse occurs very rapidly and this is used to identify the onset of crystallinity. The kinetics of crystallization after the onset point is usually described by the Avrami equation [9].

The three measurements in Fig. 3 were acquired at 40°C and water activities of 0.58 $a_w$ in Fig. 3a, 0.48 $a_w$ in Fig. 3b and 0.39 $a_w$ in Fig. 3c. The *measurement time* to reach glass transition $t_{gm}$ is acquired at the peak of tan$\delta_p$, $t_m$ curve. The *measurement time* to reach the onset of crystal collapse is $t_{cm}$ and is acquired where the tan$\delta_p$ has a precipitous drop. At the same temperature, measurement times become longer as the $a_w$ decreases. The *glass transition time* is $t_g = t_{gm} - t_p$ and the *onset of crystallinity time* is $t_c = t_{cm} - t_p$. where $t_p$ is the preconditioning time.

*Preprints* (www.preprints.org) | NOT PEER-REVIEWED | Posted: 9 April 2018 doi:10.20944/preprints201804.0105.v1

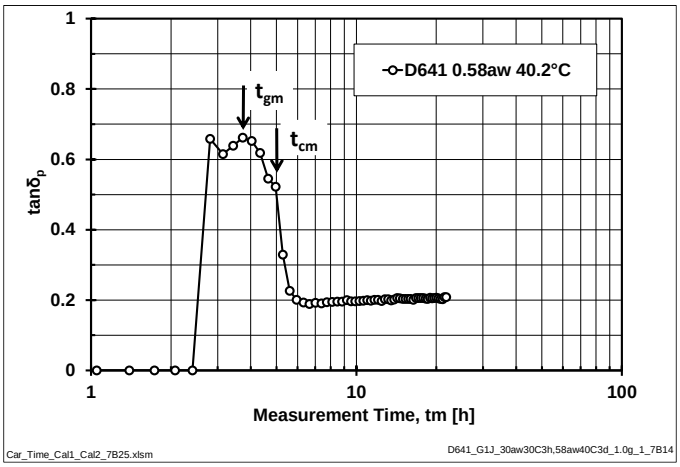


Fig. 3a. $\tan\delta_p$, $t_m$ curve at 40.2°C and 0.580 $a_w$.

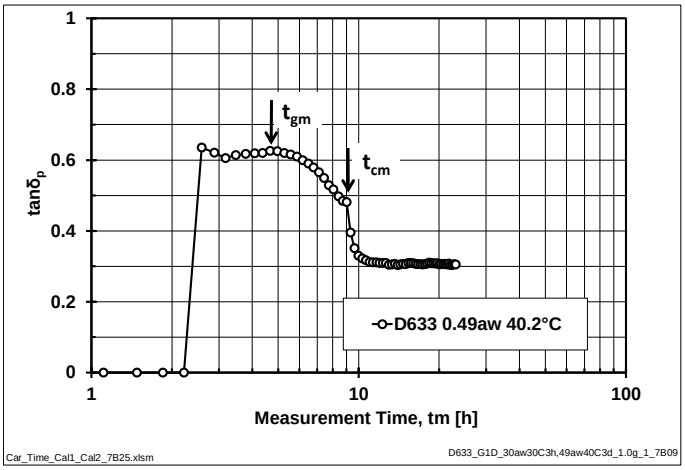


Fig. 3b. $\tan\delta_p$, $t_m$ curve at 40.2°C and 0.489 $a_w$

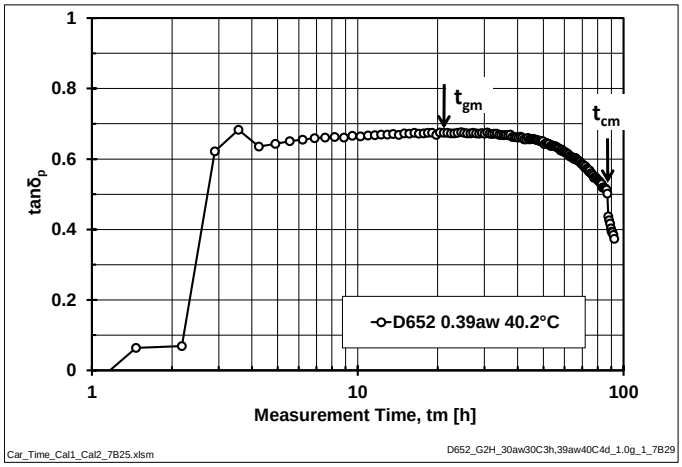


Fig. 3c. $\tan\delta_p$, $t_m$ curve at 40.1°C and 0.390 $a_w$.

Using the procedure outlined in Fig. 3, $a_w$, $t_g$ curves are shown in Fig. 4a and $a_w$, $t_c$ curves are shown in Fig. 4b at various temperatures. The data in these figures indicate that when $T$ and $a_w$ decrease, $t_g$ and $t_c$ increase. The derivation of the fitting equations is shown in the next section.

Preprints (www.preprints.org) | NOT PEER-REVIEWED | Posted: 9 April 2018 doi:10.20944/preprints201804.0105.v1

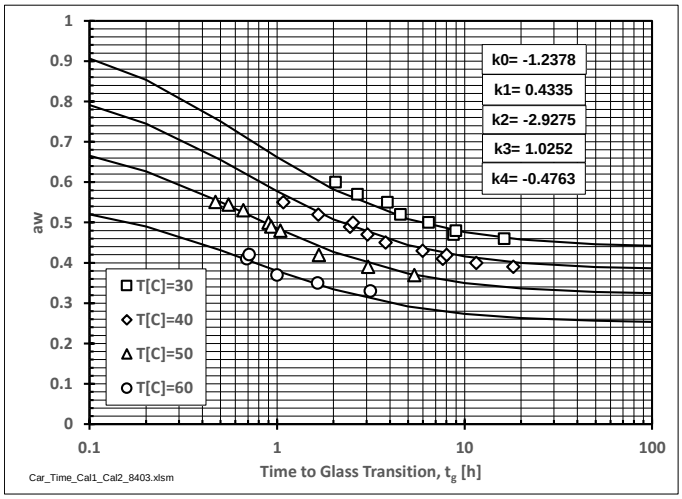


Fig. 4a. Time for glass transition at various $T$ and $a_w$ values.

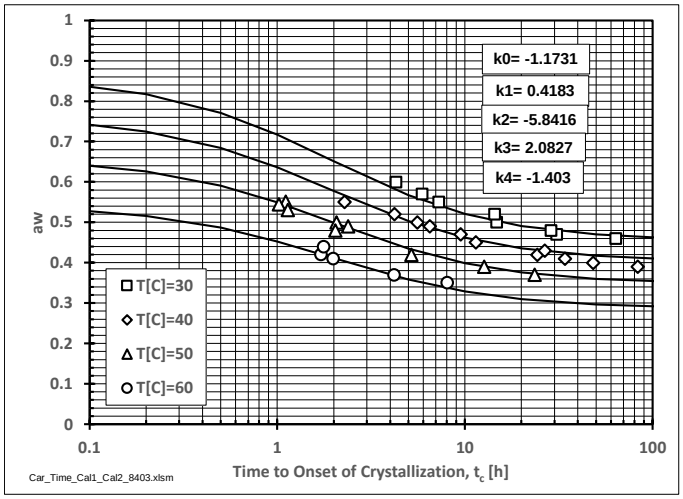


Fig. 4b. Time for onset of crystallinity at various $T$ and $a_w$ values.

**Fitting the $a_w$, $t_g$ and $a_w$, $t_c$ Curves:** The algorithm fitting the data in Fig. 4 was derived from a modification of the Arrhenius equation. The equation below shows the relationship between the time to arrive at an event such as glass transition or onset of crystallinity which is based on the ability to jump the potential barrier ΔG:

$$t = t_0 \exp(\Delta G / RT^*) \quad [1]$$

where $t_0$ is the preexponential time constant, $R$ is the Gas constant, $T^*$ is the absolute temperature and $\Delta G$ is the magnitude of the energy barrier described by:

$$\Delta G = \Delta H_0 - RT^* B a_w^2 \quad [2]$$

where $\Delta H_0$ is the barrier enthalpy, $a_w$ is the water activity which varies from 0 to 1 and $B$ is the water-activity coefficient. Notice that both $T^*$ and $a_w$ lower the potential barrier, ΔG. By taking the logarithm of Eq. 1, by approximating $\ln(t/t_0)$ with $1 - t_0/t$ and using Eq. 2 lead to a general expression. Solving for the water activity leads to the following basic equation:

Preprints (www.preprints.org) | NOT PEER-REVIEWED | Posted: 9 April 2018 doi:10.20944/preprints201804.0105.v1

$$a_w^2 = -\frac{1}{B} + \frac{\Delta H_0}{BR}\frac{1000}{T^*} + \frac{t_0 1}{Bt} = k_0 + k_1\frac{1000}{T*} + k_2\frac{1}{t} \quad [3]$$

where the *k*-coefficients represent the *B*, $\Delta H_0$ and $t_0$ parameters. The 1000 factor allows temperatures to be expressed in numbers greater than unity and it also means that $\Delta H_0$ has units of kJ/mole.

The above equation provides the framework for the fitting algorithm, but two more terms are needed to keep the above algorithm bounded as *t* and *T** go to zero. The two additional terms are included in the following general expression:

$$a_w^2 = k_0 + k_1\frac{1000}{T*} + k_2\frac{1}{t} + k_3\frac{1000}{T^*}\frac{1}{t} + k_4 a_w^2\frac{1}{t} \quad [4]$$

The terms associated with $k_3$ and $k_4$ allow for an S-shaped curve when plotting the $a_w$, *t* curve and 1000/*T**, *t* curve. The S-Shaped fitting curves can be seen in Fig. 4. The data fitting algorithm follows by rearranging Eq. 4:

$$a_w^2 - k_0 = k_1\frac{1000}{T*} + k_2\frac{1}{t} + k_3\frac{1000}{T^*}\frac{1}{t} + k_4 a_w^2\frac{1}{t} \quad [5]$$

Curve fitting was accomplished using Excel's Linest and $k_0 = k_1k_2/k_3$. This relationship was determined by setting the temperature at $t = 0$ equal to the temperature at $t = \infty$ for $a_w = 0$. The *k*-coefficients are listed in the legends of Fig. 4. The fitting curves for Fig. 4 were determined by rearranging Eq.4

$$a_w^2 = \frac{k_0 + k_1\frac{1000}{T*} + \left(k_2 + k_3\frac{1000}{T^*}\right)\frac{1}{t}}{1 - k_4\frac{1}{t}} \quad [6]$$

**Boundary Curve:** The boundary curve, in Fig. 5, delineates regions where the glass transition temperature $T_g$, $a_w$ state space and the onset of crystallinity temperature $T_c$, $a_w$ state space where the SMP is stable or unstable. The fitting curves seen in Fig. 4 are used to determine the boundary curves. Using Eq. 6 the limiting case for glass transition where $t \rightarrow \infty$ is $a_{w\infty}^2 = k_0 + k_1 1000/T*$. Using Eq. 6, the limiting case for the onset of crystallinity where $t \rightarrow 0$ is $a_{w0}^2 = (k_2 + k_3 1000/T*)k_4$. Limiting case values are listed in Table 1 and appear as the square and diamond data points in Fig. 5. The curve fitting algorithms for the curves in Fig. 5 are discussed in the next section.

Table 1. Water Activities

| | Glass-Static $t\rightarrow\infty$ | Cry-Static $t\rightarrow 0$ |
|---|---|---|
| *T*[°C] | $a_{w\infty}$ | $a_{w0}$ |
| 30 | 0.4382 | 0.8564 |
| 40 | 0.3826 | 0.7596 |
| 50 | 0.3218 | 0.6559 |
| 60 | 0.2516 | 0.5407 |

Preprints (www.preprints.org) | NOT PEER-REVIEWED | Posted: 9 April 2018 doi:10.20944/preprints201804.0105.v1

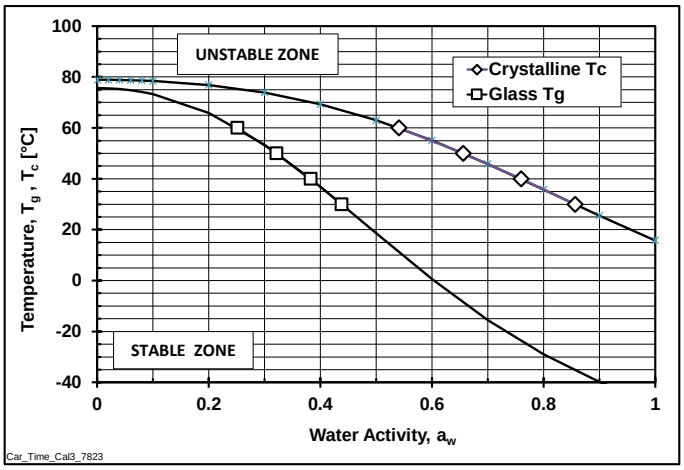


Fig. 5. Boundary curves for glass (square) and crystalline (diamond) transition.

**Fitting the Boundary Curves:** A common algorithm used to fit the data in Fig. 5 is the Gordon-Taylor (G-T) equation [9, 10]. Because the slope of the G-T equation is not zero at $a_w$ = 0, it was modified by squaring two of the $a_w$ terms shown in the following algorithm:

$$T_g = \frac{(1-a_w)T_{g0} + kT_{g1}a_w^2}{1-a_w + ka_w^2} \quad [7]$$

where $T_{g0}$, $T_{g1}$ and $k_g$ are the fitting coefficients. Taking $\partial T_g/\partial a_w|_{aw\to 0}$ demonstrates that the slope of the boundary curve is zero at $a_w$ = 0. The fitting coefficients were found from the following algorithm:

$$T_g(1-a_w) = [T_{g0}](1-a_w) + [kT_{g1}]a_w^2 + [-k]a_w^2 T_g \,. \quad [8]$$

A similar equation was written for the onset of crystallinity where the fitting coefficients are $T_{c0}$, $T_{c1}$ and $k_c$. Curve fitting was accomplished using Excel's Linest and the fitting coefficients are listed in Table 2.

Table 2. Fitting Coefficients for the Boundary Curve, Eq. 7.

| | Glass Transition | | Crystalline Transition |
|---|---|---|---|
| $T_{g0}$[°C] | 75.59 | $T_{c0}$[°C] | 78.89 |
| $T_{g1}$[°C] | -48.12 | $T_{c1}$[°C] | 15.80 |
| $k_g$ | 1.706 | $k_c$ | 0.6727 |

The initial slope of the boundary curve at $a_w$ = 0 was discussed by Sandoval and Muller [11]. They argue that the initial slope is govern by the "first sorbed water molecules". Depending on the food matrix, the initial slope can be either negative, zero or positive. In the absence of data near $a_w$ = 0, zero slope has been chosen to analyse our SMP data.

**Comparison of DSC and DRS methods:** A comparison of the DSC and DRS is shown in Fig. 6. To compare results, the SMP samples must be as identical as possible. All the samples were spray dried and have essentially sample lactose content as seen in Table 3. However, they were produced over a twelve-year period. Major differences between the methods are heating rates and sample environment. The heating rates for the DSC samples are either 3 or 5 °C/min; whereas, the DRS has zero heating rate. The sample environment for the DSC samples involves pre-equilibrated samples at selected $a_w$ values using saturated salts that are subsequently hermetically sealed. Thus, the overhead $a_w$ is not controlled in this sealed environment. In the DRS method the overhead $a_w$ environment is under active control. As seen in Fig. 6, the DSC method has a smaller stable zone than the DRS method. Given the differences between the methods, it is difficult to find a specific reason for the difference although the heating rate seems to be the major factor.

Preprints (www.preprints.org) | NOT PEER-REVIEWED | Posted: 9 April 2018 doi:10.20944/preprints201804.0105.v1

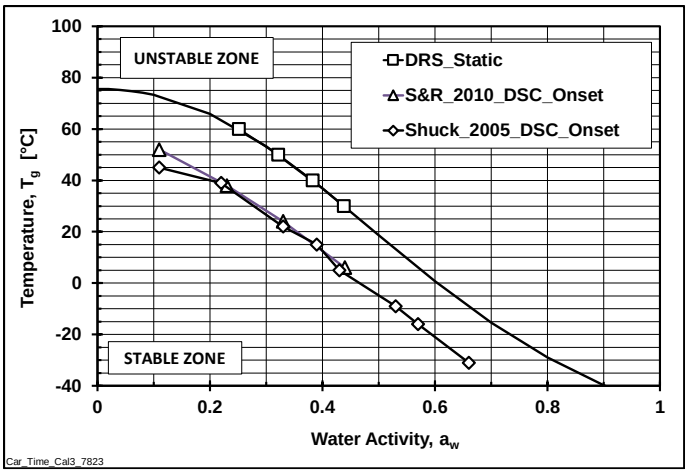


Fig. 6. Comparison of DSC and DRS measurements.

Table 3. DSC and DRS Method Attributes.

| Reference | Method | Production Date | SMP Lactose Content [%] | Heating Rate [°C/min] | Sample Environment |
|---|---|---|---|---|---|
| Schuck [12] | DSC | ~2005 | 55 | 5 | Static |
| Silalai-Roos [4] | DSC | ~2010 | 48 | 3 | Static |
| This Work | DRS | 2017 | 53 | 0 | Active |

**Enthalpy ($\Delta H_0$) and Water Activity Parameters ($B$):** The parameters were calculated using the basic equation, Eq. 3. That is, $B = -1/k_0$, $\Delta H_0 = -k_1 R/k_0$ and $t_0 = -k_2/k_0$ where the $k$-coefficients are listed in the legends of Fig. 4. Values for the parameters are listed in Table 4. Values for the enthalpies listed in Table 4 agree with those mentioned by Schuck [15]. For weaker hydrogen bonds he mentions enthalpies have values between 1 to 3 kJ/mol. The negative values for $t_0$ are artifacts resulting from using the basic equation, Eq. 3.

Table 4. $B$ and $\Delta H_0$ Parameters

| Parameter | Glass Transition | Onset of Crystallinity |
|---|---|---|
| B [na] | 0.8079 | 0.8524 |
| $\Delta H_0$ [kJ/mol] | 2.9117 | 2.9646 |
| $t_0$ [h] | -2.3651 | -4.9796 |

**Discussion:** The DRS measured values are acquired at constant $T$ and $a_w$. The DSC measured values are acquired by keep the $a_w$ quasi-constant and ramping temperature. In fact, DSC measurement cannot be acquired at constant temperature [13] for the magnitude of the heat signal is heating rate dependent. However, DSC measurements can be extrapolated to zero heating rate but this will result is a lower value for $T_g$ [13, 14]. The results in Fig. 6 shown that the boundary curve for DSC method carves out a smaller stable zone than for the DRS method. This is important when using the boundary curve to predict shelf life. For example, at 25°C the critical water activity is 0.31 $a_w$; whereas, it is 0.48 $a_w$ for the DRS method. Thus, there is a need to resolve differences between the DRS and DSC methods.

Using the DRS method the onset of crystallinity is determined from a catastrophic change in measured properties. This change is coupled with lactose content. Results presented here are based on SMP lactose content near 50%. This collapse has been observed in a wide number of samples with approximately 50% lactose content including infant formula. The author has observed the catastrophic change in sample with 72% lactose content but has not seen the catastrophic change in samples with 15% lactose content.

**Acknowledgement:** The author is pleased to have three world-class instruments. The humidity and temperature control system was designed by Gaylon Campbell. This system is combined with an impedance spectrometer and used to collect dielectric data. One of these instruments was assembled by Spencer Logo-Echeverria; the others are early prototypes. The help of Ken Byers with humidity control system and Fred Lionetti with pre-processor software. Thanks to Greg Chandler, Darigold, Inc. for supplying the SMP samples. The data is found in file DGSMP_7819.xlsm and the analysis used file Car_Time_Cal1_Cal2_7B25.xlsm.

**References:**

1. Schuck, P. Implications of Non-Equilibrium States and Glass Transitions in Dairy Powders, B. Bhandari and Y. Roos, Eds. *Non-Equilibrium States and Glass Transitions in Foods*; Elsevier, Inc., Duxford, UK; 2017, p.303.
2. United Nations, Department of Economics and Social Affairs, Population Division, "World Population Prospects, The 2017 Revision".
3. Meyer. D.; American Dairy Products Institute, private communication.
4. Salalai, N.; Roos, Y. H.; Roles of Water and Solid Composition in the Control of Glass Transition and Stickiness of Milk Powders, J. Food Science; 2010; 75, E285-E296.
5. Clark, Z.; Paterson, A. H. J.; Joe, R.; and Mcleod, J. S.; Amorphous lactose crystallisation kinetics, International Dairy Journal, 2016; Volume 56, pp. 22-28.
6. Dean, R. N.; Rane, A. K.; Baginski, M. E.; Richard, J.; Hartzog, Z.; and Elton, D. J.; A Capacitive Fringing Field Sensor Design for Moisture Measurement Based on Printed Circuit Board Technology, IEEE Trans. Instrum. Meas, 2012; volume 61, no. 4, 1105-1112, 2012.
7. Buehler, M. G.; Kindle, M. L.; Carter, B. P.; Using Dielectric Relaxation Spectroscopy to Characterize the Glass Transition Time of Polydextrose, J. Food Science, 2015;Volume 80, pp. E1243–E1252.
8. Salalai, N.; Roos, Y. H.; Dielectric and Mechanical Properties Around Glass Transition of Milk Powders, Drying Technology, 2010; Volume 28, pp. 1044-1054.
9. Tells, V. R. N.; Tonon, R. V.; The Effects of Non-Equilibrium States and Storage Conditions on Glass Transitions in Foods, *Non-Equilibrium States and Glass Transitions in Foods*, Bhandari, B.; Roos, Y. H. Eds; Elsevier-Woodhead Publishing, Duxford, UK, 2017; p. 382.
10. Gordon, M.; Taylor, J. S. Ideal copolymers and the second-order transition of synthetic rubbers. I. Non-crystalline copolymers. J. Appl. Chem. 1952; Volume 2, 493-500.
11. Sandoval A. J.; Muller, A. J.; Implications of Non-Equilibrium State Glass Transitions on Carbohydrate Polymers, *Non-Equilibrium States and Glass Transitions in Foods*, Bhandari, B.; Roos, Y. H. Eds; Elsevier-Woodhead Publishing, Duxford, UK, 2017; p. 199.
12. Schuck, P.; Blanchard, E.; Dolivet, A.; Mejean, S.; Onillon, E.; Jeantet, R.; Water activity and glass transition in dairy ingredients, Lait, 2005; Volume 85, 295-304.
13. Hohne, G.; Hemminger, W.; Flammersheim, H.-J.; Differential Scanning Calorimetry, Springer-Verlog Berlin, 1996; pp. 34, 56.
14. Buehler, M. G.; Methods of Measurement of Non-Equilibrium State Glass Transitions on Carbohydrate Polymers, Bhandari, B.; Roos, Y. H. Eds; Elsevier-Woodhead Publishing, Duxford, UK, 2017; Fig. 1.16 p. 19.
15. Schuck, P.; Implications of Non-Equilibrium States and Glass Transitions in Dairy Powders, Bhandari, B.; Roos, Y. H. Eds; Elsevier-Woodhead Publishing, Duxford, UK, 2017; p. 320.